nature geoscience

LETTERS

PUBLISHED ONLINE: 18 MAY 2015 | DOI: 10.1038/NGEO2438

Pacific origin of the abrupt increase in Indian Ocean heat content during the warming hiatus

Sang-Ki Lee[1,2]*, Wonsun Park[3], Molly O. Baringer[2], Arnold L. Gordon[4], Bruce Huber[4] and Yanyun Liu[1,2]

Global mean surface warming has stalled since the end of the twentieth century[1,2], but the net radiation imbalance at the top of the atmosphere continues to suggest an increasingly warming planet. This apparent contradiction has been reconciled by an anomalous heat flux into the ocean[3–8], induced by a shift towards a La Niña-like state with cold sea surface temperatures in the eastern tropical Pacific over the past decade or so. A significant portion of the heat missing from the atmosphere is therefore expected to be stored in the Pacific Ocean. However, *in situ* hydrographic records indicate that Pacific Ocean heat content has been decreasing[9]. Here, we analyse observations along with simulations from a global ocean–sea ice model to track the pathway of heat. We find that the enhanced heat uptake by the Pacific Ocean has been compensated by an increased heat transport from the Pacific Ocean to the Indian Ocean, carried by the Indonesian throughflow. As a result, Indian Ocean heat content has increased abruptly, which accounts for more than 70% of the global ocean heat gain in the upper 700 m during the past decade. We conclude that the Indian Ocean has become increasingly important in modulating global climate variability.

Several studies have linked the recent pause in the rise of the global mean surface air temperature to a shift towards a more La Niña-like state in the tropical Pacific Ocean, triggered by a series of long-lasting La Niña events since the end of the twentieth century[3–8]. The resulting La Niña-like state has lifted relatively cold equatorial thermocline water towards the surface, producing persistently cold sea surface temperature (SST) anomalies in the eastern Pacific. Cold SST anomalies are associated with reductions in surface upward longwave radiation and latent heat flux to the atmosphere[10]. Thus, the net surface heat flux into the tropical Pacific Ocean increased sharply in the 2000s (refs 6,8). In addition, the cold SST anomalies and associated cooling of the atmosphere in the equatorial Pacific could also force extra-tropical stationary waves to remotely enhance heat flux into the Atlantic and Southern oceans[11]. Two independent studies have suggested that surface heat uptake indeed increased in the Atlantic and Southern oceans during the 2000s, leading to a downward flux of the upper ocean's heat into the deeper ocean[8,12].

In agreement with enhanced surface heat uptake in the Pacific, Atlantic and Southern oceans, the global ocean heat content in the upper 700 m (OHC_{700}) increased strongly during 2003–2012 (Fig. 1a) at a rate of about 2.9×10^{22} J per decade[9,12,13] (see Supplementary Information 1). However, there are significant differences in recent OHC_{700} changes between the major ocean basins, particularly the Pacific and Indian oceans (Fig. 1b,c; see also Supplementary Information 1 and 2). For the Pacific Ocean, OHC_{700} decreased during 2003–2012, in spite of the increased surface heat uptake in the eastern Pacific[6,8] (Fig. 1c). In sharp contrast, the OHC_{700} of the Indian Ocean increased abruptly during 2003–2012, at a rate of about 2.1×10^{22} J per decade (Fig. 1b), accounting for more than 70% of the global ocean heat gain in the upper 700 m during that period. This suggests that a significant portion of the heat missing from the atmosphere now resides in the upper 700 m of the Indian Ocean, with little explanation. Given that the OHC_{700} in the Indian Ocean did not increase during 1971–2000 (Fig. 1b), and that the Indian Ocean (north of 34° S) covers only 12% of the global sea ice-free ocean surface area, the marked increase of the Indian OHC_{700} is striking.

Hence, a significant gap exists in our understanding of the heat missing from the atmosphere and its distribution between the different ocean basins. In particular, the difference between the Pacific and Indian oceans in their recent warming trends needs to be reconciled, which is the main objective of the present study. To do so, we use a series of global ocean–sea ice general circulation model simulations forced with the bias-corrected twentieth century reanalysis surface fluxes[14] (Methods; see also Supplementary Information 3). Two sets of six-member ensemble experiments are used: a control experiment forced with real-time surface flux fields and a reference experiment forced with climatological surface flux fields (Methods; see also Supplementary Information 4).

The results from these ensemble experiments can be summarized as two sets of global OHC_{700} time series (Fig. 1a). The simulated global OHC_{700} from the control experiment follows the time variability of *in situ* observations since the 1950s (ref. 9) reasonably well. Note that there is no apparent drift of the global OHC_{700} in the reference experiment. The dominant forcing terms of the recent hiatus can be determined by comparing the global ocean heat budget terms averaged for the 1971–2000 period with the 2003–2012 period, with both periods computed as anomalies relative to the reference experiment (Fig. 1d). The heat budget indicates that the simulated global OHC_{700} increase since 1971 was largely driven by an increased downward longwave radiative heat flux, consistent with the thermodynamic effects of increased anthropogenic greenhouse gases in the atmosphere. This flux has accelerated in the most recent decade (that is, 2003–2012) and is damped by both an increased upward longwave radiative heat flux and latent heat flux.

The Indian OHC_{700} shows very weak to no increase, in contrast to the strong global OHC_{700} increase during 1971–2000 in both the observational estimates and the control simulation (Fig. 1b). During the 2000s, however, observations show an abrupt increase,

[1]Cooperative Institute for Marine and Atmospheric Studies, University of Miami, Miami, Florida 33149, USA. [2]Atlantic Oceanographic and Meteorological Laboratory, NOAA, Miami, Florida 33149, USA. [3]GEOMAR Helmholtz Centre for Ocean Research Kiel, D-24105 Kiel, Germany. [4]Lamont-Doherty Earth Observatory, Earth Institute at Columbia University, Palisades, New York 10964, USA. *e-mail: Sang-Ki.Lee@noaa.gov

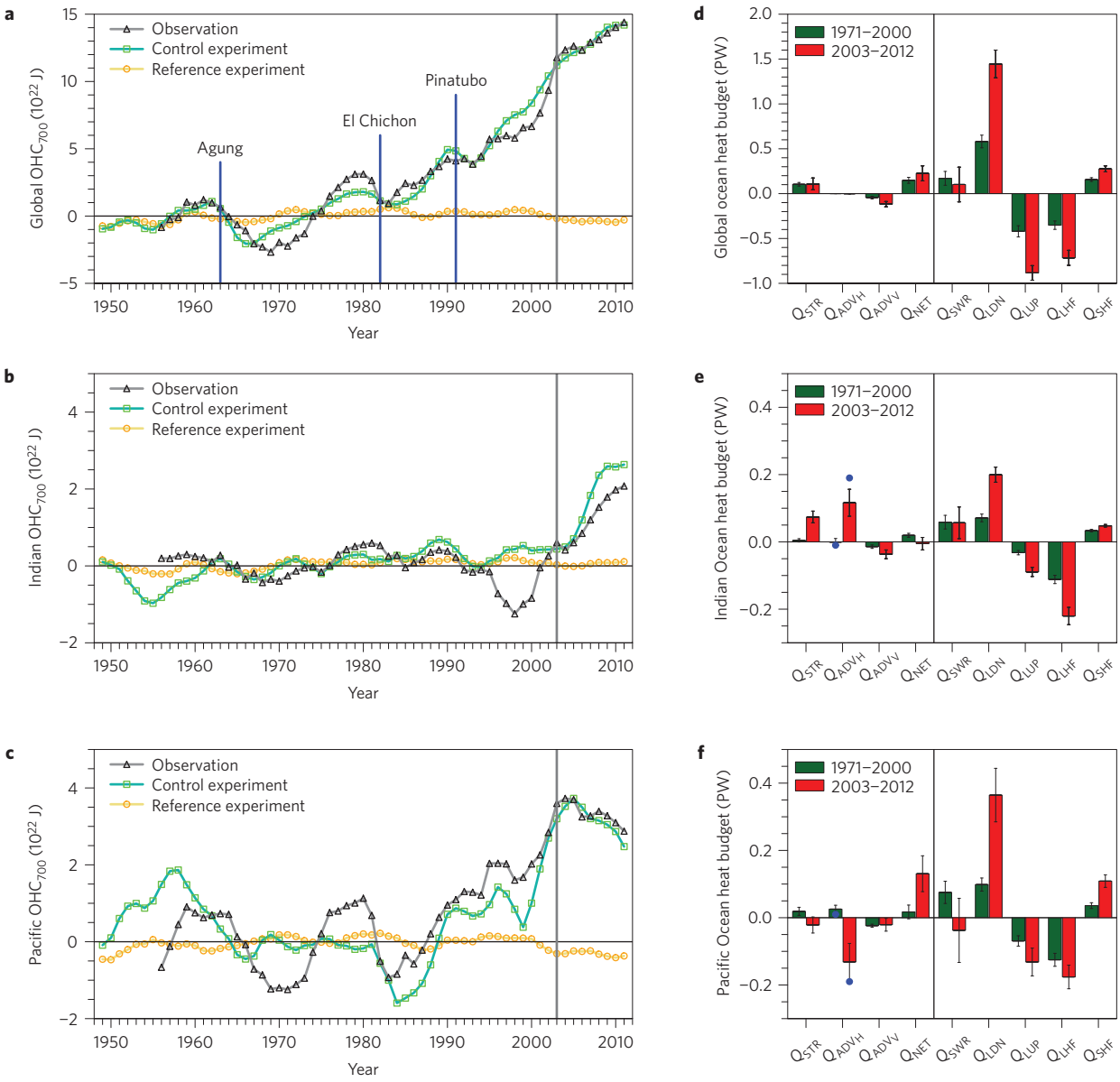

Figure 1 | OHC_{700} and heat budget for the global ocean, and the Indian and Pacific oceans. a–c, Time series of OHC_{700} for the global (**a**), Indian (**b**) and Pacific (**c**) oceans derived from the control and reference experiments and observations[9]. **d–f**, Storage rate (Q_{STR}), horizontal and vertical advections (Q_{ADV_H} and Q_{ADV_V}), net surface heat flux (Q_{NET}), shortwave radiation (Q_{SWR}), downward and upward longwave radiations (Q_{LDN} and Q_{LUP}), and latent and sensible heat fluxes (Q_{LHF} and Q_{SHF}) for the global (**d**), Indian (**e**) and Pacific (**f**) oceans derived from the control experiment relative to the reference experiment are averaged for the 1971–2000 (green bars) and 2003–2012 periods (red bars). The error bars show the 90% confidence levels derived from the six-member ensemble runs. The blue circles in **e**,**f** indicate the values for inter-ocean heat transport via the Indonesian passages.

which was reproduced in the control simulation, although the control simulation did not capture a short-term decrease during the late 1990s. Surprisingly, the heat budget analysis shows that the abrupt increase of the Indian OHC_{700} during 2003–2012 was not due to surface heating, but rather due almost entirely to horizontal advective heat convergence (Fig. 1e). Further heat budget analysis indicates that inter-ocean heat transport from the Pacific Ocean to the Indian Ocean via the Indonesian passages was the main cause of the increased Indian OHC_{700}; it greatly increased during 2003–2012, overcompensating for the slightly increased southward heat transport from the Indian Ocean to the Southern Ocean across 34° S (see Supplementary Information 5 for detail).

These changes in the Indian Ocean are supported by complementary changes in the Pacific Ocean. The net surface heat flux into the Pacific Ocean increased greatly during 2003–2012 (Fig. 1f), consistent with the La Niña-like condition across the Pacific Ocean[6,8]. However, the anomalous surface heat uptake was completely masked by horizontal advective heat divergence, which was mainly linked to the increased heat transport to the Indian Ocean (see Supplementary Information 5 for detail). Thus, the Pacific OHC_{700} did not increase, but instead shows a slight decrease during this period.

Given the important role played by the inter-ocean heat transport via the Indonesian passages in the Indian and Pacific OHC_{700} changes, a closer examination of the Indonesian throughflow (ITF) is warranted (Fig. 2). During 2003–2012, the ITF heat transport increased from −0.95 PW in the reference experiment to −1.14 PW in the control experiment, yielding an approximately −0.19 PW of increase into the Indian Ocean (Fig. 2a; see also

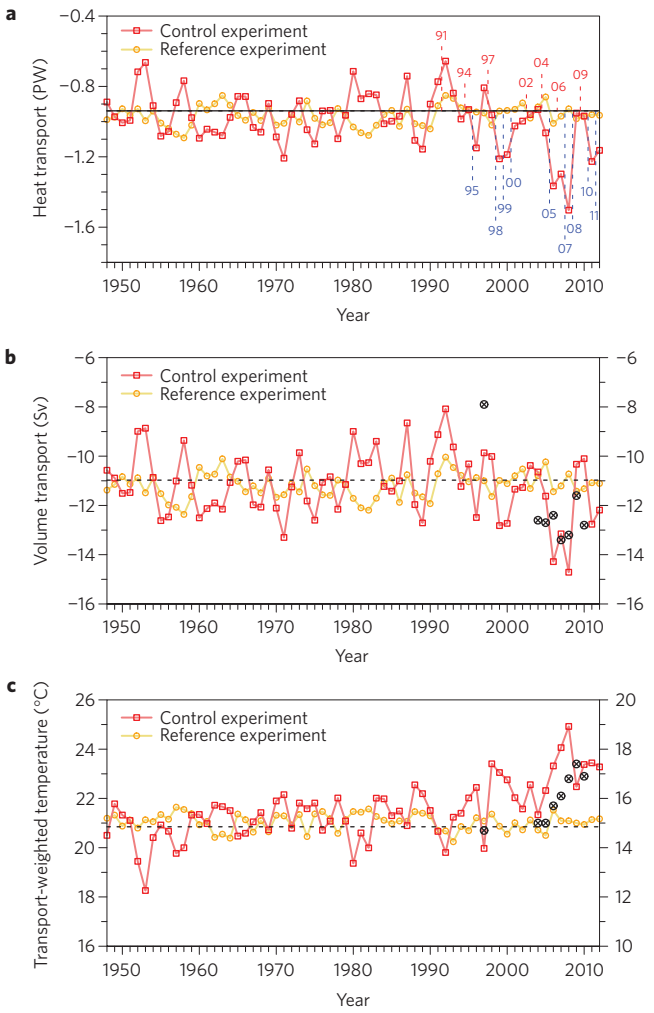

Figure 2 | ITF heat and volume transports and transport-weighted temperature in the upper 700 m. a–c, Time series of the ITF heat transport (**a**), ITF volume transport (**b**) and ITF transport-weighted temperature (**c**) derived from the control and reference experiments. The two digit numbers in **a** indicate the onset years of El Niño (red) and La Niña (blue) events since 1990. *In situ* measurements of volume transport and transport-weighted temperature across the Makassar Strait[15–17] (crossed circles) are also shown in **b** and **c** respectively (right-hand *y* axis).

Supplementary Information 5; the negative indicates transport from the Pacific Ocean to the Indian Ocean). Both the ITF volume transport and the ITF transport-weighted temperature, which is simply the ITF heat transport divided by the ITF volume transport, contributed positively to the ITF heat transport increase (Fig. 2b,c).

The flow through the Makassar Strait accounts for more than 85% of the total ITF volume transport within the upper 700 m, and hence is a useful proxy for the total ITF (ref. 15). *In situ* observations of the transports in the Makassar Strait (Methods) also indicate that both the volume transport and transport-weighted temperature across the Strait were much larger during 2004–2010 than in 1997 (refs 15–17; Fig. 2b,c). Although the simulated ITF volume transport and transport-weighted temperature in the upper 700 m did not match year-to-year with the *in situ* measurements, they were generally much larger in 2006–2008 than in 1997, in overall agreement with the *in situ* measurements.

It has been shown that the ITF volume transport is mainly dominated by interannual variability associated with El Niño/Southern Oscillation (ENSO; refs 18,19). Indeed, in the control experiment, the reduced ITF volume transport during 1997–1998 coincides with the 1997–1998 El Niño. Conversely, the large increase in the ITF volume transport during 2006–2008 coincides with the three near-consecutive La Niña events, namely the 2005–2006, 2007–2008 and 2008–2009 events, which contributed significantly to the recent La Niña-like state in the Pacific Ocean. Observational evidence is consistent with the reduced ITF during the 1997–1998 El Niño and the increased ITF during the series of La Niña events from 2006 to 2008. Therefore, it is logical to conclude that a series of long-lasting La Niña events without strong and intervening El Niño events has led to the increased ITF heat transport in the 2000s.

A closer look at the distribution of the changes in sea surface height (SSH) and heat transport during 2003–2012 is shown in Fig. 3a. The anomalous zonal wind stress[14] averaged over the Pacific (0°–40° N), Indian (34° S–0°) and Southern (50° S–34° S) oceans during the same period is shown in Fig. 3b. The anomalous easterlies and associated wind stress curl anomalies over the South Indian Ocean produced negative SSH anomalies between 10° S and 0° and positive SSH anomalies between 25° S and 10° S over the South Indian Ocean[20,21] (Fig. 3a). Similarly, the negative wind stress curl anomalies over the tropical North Pacific associated with the anomalous easterlies (0°–15° N) and westerlies (15°–30° N) produced positive SSH anomalies in the tropical northwestern Pacific[22]. Therefore, a strong anomalous pressure gradient formed from the tropical northwestern Pacific to the tropical South Indian Ocean, and thus increased the ITF volume and heat transports. In response to the anomalous surface winds, both the North Equatorial Current in the Pacific and the South Equatorial Current in the Indian Ocean strengthened, aiding the inter-ocean heat and volume transports. Further sensitivity experiments (Methods) confirm that the anomalous surface wind fields in the Pacific and Indian oceans are the key to increasing the ITF heat transport in the control experiment during the 2000s, as summarized in Fig. 4 (see Supplementary Information 6 for detail).

During a typical La Niña event, deep tropical convection strengthens over the Maritime Continent, producing anomalous low-level convergence; thus, the easterlies should increase over the western tropical Pacific Ocean and decrease over the eastern tropical Indian Ocean[23]. In agreement with this, the composite mean zonal wind stress for the La Niña years of 1971, 1975, 1989, 1996 and 1999, during which the simulated ITF heat transports increased by more than one standard deviation, increased in the equatorial North Pacific and decreased in the equatorial South Indian Ocean (Fig. 3b). This suggests that the anomalous easterlies over the tropical South Indian Ocean (Fig. 3b) may not be linked to the La Niña-like conditions in the Pacific Ocean. Among others, one hypothesis is that the persistent increase of the SSTs over the tropical Indian Ocean since the 1960s has invigorated the regional Hadley circulation over the Indian Ocean, thus increasing the easterlies in the tropical South Indian Ocean[21].

The ITF is an important component of the global thermohaline circulation[24], often referred to as the ocean conveyor belt[25]. If the ITF heat transport remains strong in the next decade, then heat will continue to accumulate in the Indian Ocean which may then be projected into the Atlantic Ocean via Agulhas leakage, another important component of the global thermohaline circulation. This will further increase Atlantic Ocean heat content, which has already increased substantially since the mid-twentieth century[26]. As such, *in situ* monitoring of the volume and heat transports across the Makassar Strait into the Indian Ocean and the Agulhas leakage corridor into the South Atlantic Ocean are vital for our understanding of the distribution of the energy imbalance in the

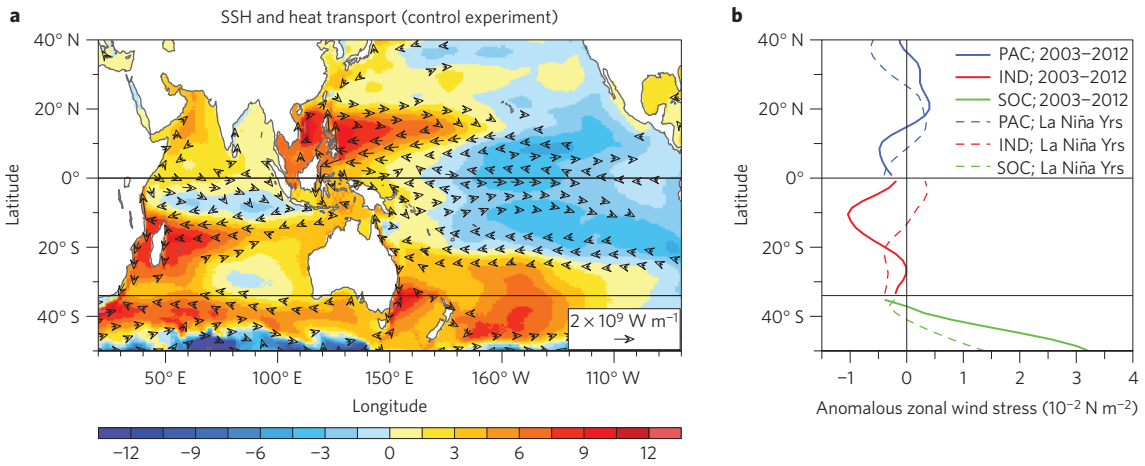

Figure 3 | Sea surface height, heat transport and zonal wind stress. a, Sea surface height (cm, colour shading) and heat transport in the upper 700 m (arrows) during 2003–2012 derived from the control experiment relative to the reference experiment. **b**, Anomalous zonal wind stress from the twentieth century reanalysis[14] averaged over the Pacific (0°–40° N), Indian (34° S–0°) and Southern (50°–34° S) oceans for 2003–2012 (solid lines) and the composite mean of the La Niña years of 1971, 1975, 1989, 1996 and 1999 (dashed lines).

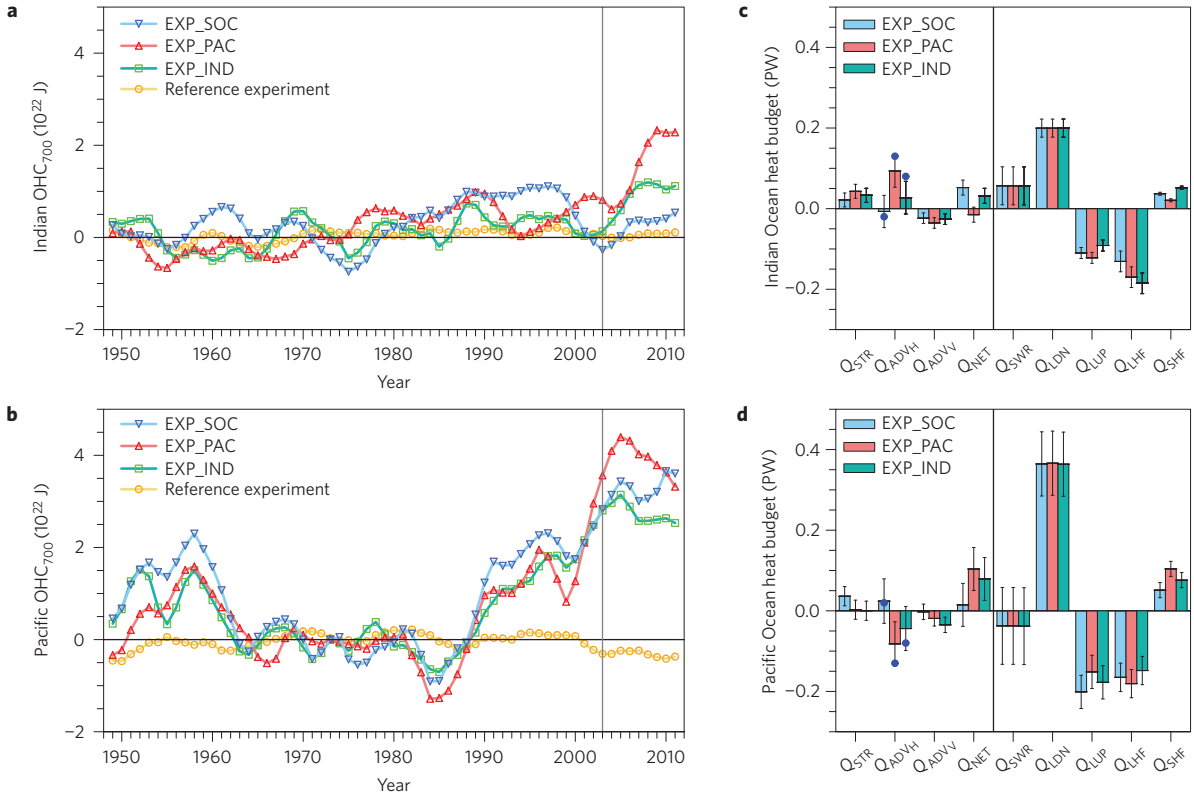

Figure 4 | OHC_{700} and heat budget for three sensitivity experiments. a,**b**, Time series of OHC_{700} for the Indian (**a**) and Pacific (**b**) oceans derived from EXP_SOC, EXP_PAC, EXP_IND, and the reference experiment. **c**,**d**, Heat budget terms for the Indian (**c**) and Pacific (**d**) oceans derived from EXP_SOC, EXP_PAC, and EXP_IND relative to the reference experiment are averaged for 2003–2012. The error bars show the 90% confidence levels derived from the six-member ensemble runs. The blue circles in **c**,**d** indicate the values for inter-ocean heat transport via the Indonesian passages. EXP_SOC, EXP_PAC and EXP_IND are identical to the control experiment except that real-time winds were applied only over the Southern, Pacific and Indian oceans, respectively. Inter-ocean heat transport increased in both EXP_PAC and EXP_IND but was almost unchanged in EXP_SOC.

Earth system, which is likely to continue throughout the twenty-first century.

Methods

Methods and any associated references are available in the online version of the paper.

Received 27 January 2015; accepted 10 April 2015; published online 18 May 2015

References

1. Loeb, N. G. *et al.* Observed changes in top-of-the-atmosphere radiation and upper-ocean heating consistent within uncertainty. *Nature Geosci.* **5,** 110–113 (2012).

2. Allan, R. P. *et al.* Changes in global net radiative imbalance 1985–2012. *Geophys. Res. Lett.* **41,** 5588–5597 (2014).
3. Meehl, G. A., Arblaster, J. M., Fasullo, J. Y., Hu, A. & Trenberth, K. E. Model-based evidence of deep ocean heat uptake during surface temperature hiatus periods. *Nature Clim. Change* **1,** 360–364 (2011).
4. Kosaka, Y. & Xie, S-P. Recent global-warming hiatus tied to equatorial Pacific surface cooling. *Nature* **501,** 403–407 (2013).
5. Trenberth, K. E. & Fasullo, J. T. An apparent hiatus in global warming? *Earth's Future* **1,** 19–32 (2013).
6. England, M. H. *et al.* Recent intensification of wind-driven circulation in the Pacific and the ongoing warming hiatus. *Nature Clim. Change* **4,** 222–227 (2014).
7. Maher, N., Sen Gupta, A. & England, M. H. Drivers of decadal hiatus periods in the 20th and 21st centuries. *Geophys. Res. Lett.* **41,** 5978–5986 (2014).
8. Drijfhout, S. S. *et al.* Surface warming hiatus caused by increased heat uptake across multiple ocean basins. *Geophys. Res. Lett.* **41,** 7868–7874 (2014).
9. Levitus, S. *et al.* Global ocean heat content 1955–2008 in light of recently revealed instrumentation problems. *Geophys. Res. Lett.* **36,** L07608 (2009).
10. Csanady, G. T. Warm water mass formation. *J. Phys. Oceanogr.* **14,** 264–275 (1984).
11. Trenberth, K. E., Fasullo, J. T., Branstator, G. & Phillips, A. S. Seasonal aspects of the recent pause in surface warming. *Nature Clim. Change* **4,** 911–916 (2014).
12. Chen, X. & Tung, K-K. Varying planetary heat sink led to global-warming slowdown and acceleration. *Science* **345,** 897–903 (2014).
13. Trenberth, K. E., Fasullo, J. T. & Balmaseda, M. A. Earth's energy imbalance. *J. Clim.* **27,** 3129–3144 (2014).
14. Compo, G. P. *et al.* The twentieth century reanalysis project. *Q. J. R. Meteorol. Soc.* **137,** 1–28 (2011).
15. Gordon, A. L. *et al.* Makassar Strait throughflow, 2004 to 2006. *Geophys. Res. Lett.* **35,** L24605 (2008).
16. Gordon, A. L. *et al.* The Indonesian throughflow during 2004–2006 as observed by the INSTANT program. *Dyn. Atmos. Oceans* **50,** 115–128 (2010).
17. Susanto, R. D., Ffield, A., Gordon, A. L. & Adi, T. R. Variability of Indonesian throughflow within Makassar Strait, 2004–2009. *J. Geophys. Res.* **117,** C09013 (2012).
18. Meyers, G. Variation of Indonesian throughflow and the El Niño–Southern Oscillation. *J. Geophys. Res.* **101,** 12255–12263 (1996).
19. England, M. H. & Huang, F. On the interannual variability of the Indonesian throughflow and its linkage with ENSO. *J. Clim.* **18,** 1435–1444 (2005).
20. Lee, T. & McPhaden, M. J. Decadal phase change in large-scale sea level and winds in the Indo-Pacific region at the end of the 20th century. *Geophys. Res. Lett.* **35,** L01605 (2008).
21. Han, W. *et al.* Patterns of Indian Ocean sea-level change in a warming climate. *Nature Geosci.* **3,** 546–550 (2010).
22. Han, W. *et al.* Intensification of decadal and multi-decadal sea level variability in the western tropical Pacific during recent decades. *Clim. Dynam.* **43,** 1357–1379 (2014).
23. Sprintall, J. & Révelard, A. The Indonesian throughflow response to Indo-Pacific climate variability. *J. Geophys. Res.* **119,** 1161–1175 (2014).
24. Gordon, A. L. Interocean exchange of thermocline water. *J. Geophys. Res.* **91,** 5037–5046 (1986).
25. Broecker, W. S. The biggest chill. *Nature Hist.* **96,** 74–82 (1987).
26. Lee, S-K. *et al.* What caused the significant increase in Atlantic Ocean heat content since the mid-20th century? *Geophys. Res. Lett.* **38,** L17607 (2011).

Acknowledgements

This work was supported by the base funding of the NOAA AOML, and by the NOAA Climate Program Office. S-K.L. acknowledges constructive comments from G. Foltz and the editorial assistance of G. Derr, L. Johns and S. Jones. W.P. acknowledges support from the GEOMAR Helmholtz Centre for Ocean Research Kiel. A.L.G. and B.H. acknowledge funding for the Makassar Strait throughflow time series provided under CICAR award number NA08OAR4320754 from NOAA. Lamont-Doherty Earth Observatory contribution number 7888.

Author contributions

S-K.L. conceived the study and wrote the initial draft of the paper. S-K.L. designed and performed the experiments. S-K.L., W.P., M.O.B. and A.L.G. contributed significantly to the discussion and interpretation of results and writing of the paper. A.L.G. and B.H. analysed the Makassar Strait mooring data. Y.L. assisted in the analysis.

Additional information

Supplementary information is available in the online version of the paper. Reprints and permissions information is available online at www.nature.com/reprints. Correspondence and requests for materials should be addressed to S-K.L.

Competing financial interests

The authors declare no competing financial interests.

Methods

Model. The global ocean–sea ice coupled model of the NCAR Community Earth System Model version 1 (CESM1; ref. 27) forced with the bias-corrected twentieth century reanalysis (20CR) surface flux variables[14] (see Supplementary Information 3) is used as the primary tool in this study. The ocean model is divided into 60 vertical levels. Both the ocean and sea ice models have 360 longitudes and 384 latitudes on a displaced pole grid, with a longitudinal resolution of about 1.0° and a variable latitudinal resolution of approximately 0.3° near the equator. An important advancement in CESM1 from earlier versions is the specification of a spatially variable coefficient in the Gent and McWilliams eddy parameterization, rather than a constant value; the ocean response to increasing Southern Hemisphere winds is in reasonable agreement with experiments using ocean models with much higher resolution that do not use this eddy parameterization[28]. See ref. 27 for a more detailed description of the CESM1 ocean–sea ice model (CESM1_POP hereafter).

Spin-up and reference experiments. To spin up the CESM1_POP, the model was initialized using temperature and salinity fields obtained from the polar hydrographic climatology[29] and integrated for 400 years using the bias-corrected 20CR surface flux fields[14]. In the spin-up run and other CESM1_POP runs, the 6-hourly surface wind vectors, air temperature and specific humidity, daily shortwave and downward longwave radiative heat fluxes, and monthly precipitation rate were specified, whereas the upward longwave radiative heat flux and turbulent surface fluxes were determined interactively by using the 6-hourly surface wind speed, air temperature and specific humidity, along with the model-produced SSTs. To incorporate the impact of atmospheric noise during the spin-up, which plays a crucial role in thermohaline convection and deep-water formation in the North Atlantic sinking regions, the surface forcing fields in each model year were randomly selected from the period 1948–1977, following the spin-up methodology used in ref. 26 (see also Supplementary Information 4). In the 400 years of the CESM1_POP spin-up run, the simulated global OHC_{700} showed no sign of drift after about 200 years. Nevertheless, the 400 years of spin-up may not be long enough for deeper oceans to reach a quasi-equilibrium state, if such a state exists. Therefore, to ensure that there is no long-term model drift in the real-time experiments, the CESM1_POP spin-up run was continued for a further 600 years, which is referred to as the reference experiment. In all experiments, the CESM1_POP was forced using the bias-corrected 20CR surface flux fields, whose monthly climatologies and high-frequency variability (that is, 5-day high-pass filtered) were corrected by using the surface flux fields obtained from the common ocean–ice reference experiments version 2 (ref. 30).

Control experiment. After the spin-up run, the CESM1_POP was integrated from 1948 to 2012 using the real-time bias-corrected 20CR surface flux fields. This experiment, referred to as the control experiment, consists of six-member model integrations that were initialized with different ocean–sea ice conditions, derived from the reference experiment on the 401st, 501st, 601st, 701st, 801st and 901st model years, to represent internal ocean variability. The six-member ensemble mean of the control experiment is analysed in reference to the six-member ensemble mean of the reference experiment (that is, the ensemble mean of the 401–465, 501–565, 601–665, 701–765, 801–865 and 901–965 model years; see also Supplementary Information 5).

Three sensitivity experiments. These experiments are identical to the control experiment except that real-time surface winds were applied only over specified oceans; for the rest of the ocean, the surface wind fields in each model year were randomly selected from the 1948–1977 period (that is, reference surface wind fields), as in the spin-up and reference experiments. In the first experiment (EXP_SOC), real-time surface winds were used over the Southern Ocean south of 34° S, and the rest of the ocean was prescribed with the reference surface wind fields. In the second experiment (EXP_PAC), real-time winds were used over the Pacific Ocean, and the other oceans were prescribed with the reference surface wind fields. Similarly, in the third experiment (EXP_IND), real-time winds were used over the Indian Ocean, and the other oceans were prescribed with the reference surface wind fields. Note that, in all three experiments, the Southern Ocean was prescribed with real-time surface winds to focus on the different role of anomalous surface winds over the Pacific and Indian oceans (see also Supplementary Information 6).

***In situ* estimates of the Indonesian throughflow within the Makassar Strait.** The annual mean values of the volume transport and transport-weighted temperature across the Makassar Strait were computed for 1997 and 2004–2010 using hourly data from moorings (0–700 m) located in the Labani Channel of the Makassar Strait[15–17]. The climatological temperature profile was used for all years; it is based on all CTD stations in the vicinity of the moorings. The temperature profile varied only slightly compared to transport changes; thus, using the climatology adds only slightly to the uncertainty of the transport-weighted temperature.

Code availability. The code used to perform CESM1_POP simulations can be accessed from the National Center for Atmospheric Research's CESM1 website (http://www.cesm.ucar.edu/models/cesm1.0).

References

27. Danabasoglu, G. *et al.* The CCSM4 ocean component. *J. Clim.* **25,** 1361–1389 (2012).
28. Gent, P. R. & Danabasoglu, G. Response to increasing Southern Hemisphere winds in CCSM4. *J. Clim.* **24,** 4992–4998 (2011).
29. Steele, M., Morley, R. & Ermold, W. PHC: A global ocean hydrography with a high-quality Arctic Ocean. *J. Clim.* **14,** 2079–2087 (2001).
30. Large, W. G. & Yeager, S. G. The global climatology of an interannually varying air–sea flux data set. *Clim. Dynam.* **33,** 341–364 (2009).

nature geoscience

SUPPLEMENTARY INFORMATION

DOI: 10.1038/NGEO2438

Pacific origin of the abrupt increase in Indian Ocean heat content during the warming hiatus

Sang-Ki Lee[1,2,*], Wonsun Park[3], Molly O. Baringer[2], Arnold L. Gordon[4], Bruce Huber[4] and Yanyun Liu[1,2]

[1]Cooperative Institute for Marine and Atmospheric Studies, University of Miami, Miami, Florida 33149, USA
[2]Atlantic Oceanographic and Meteorological Laboratory, NOAA, Miami, Florida 33149, USA
[3]GEOMAR Helmholtz Centre for Ocean Research Kiel, D-24105 Kiel, Germany
[4]Lamont-Doherty Earth Observatory, Earth Institute at Columbia University, Palisades, New York 10964, USA

Table of Contents

DOI: 10.1038/NGEO2438

S.I.1. Discussion on the World Ocean Atlas 2013

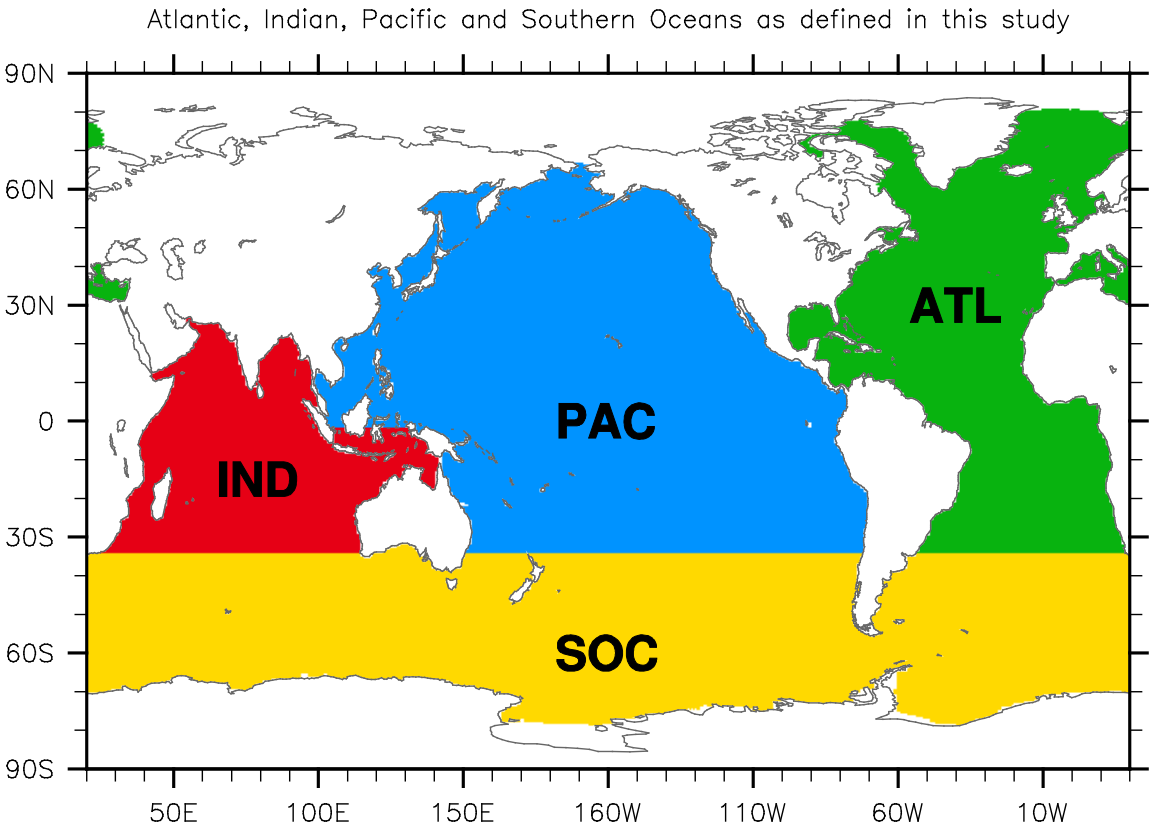

Figure S1. Four major ocean basins defined in this study. The Atlantic Ocean (ATL) includes the Mediterranean Sea and the Labrador Sea. The Southern Ocean (SOC) is directly connected to the Atlantic, Pacific and Indian Oceans at 34°S. The Indian Ocean (IND) and the Pacific Ocean (PAC) are directly connected via the Indonesian passages across 1.6°S. The contribution of the Arctic Sea on the global ocean heat change is very small thus not discussed in this study.

The World Ocean Atlas 2013 (WOA13)[1] was used to compute OHC_{700} for the global ocean, and for the Atlantic, Pacific, Indian and Southern Oceans (Fig. S1). The rates of OHC_{700} change for the global ocean, and for the Indian, Pacific, Atlantic and Southern Oceans, computed from WOA13, are shown in Table S1.

Table S1. Rates of OHC_{700} change for the global ocean and the four major ocean basins. The rates of OHC_{700} change for the global ocean, and for the Indian, Pacific, Atlantic and Southern Oceans, derived from WOA13, are shown for the periods of 1971-2000 and 2003-2012. The unit is 10^{22} J per decade.

Periods	Global Ocean	Indian Ocean	Pacific Ocean	Atlantic Ocean	Southern Ocean
1971-2000	2.8	-0.2	0.9	1.3	0.6
2003-2012	2.9	2.1	-0.4	-0.3	1.5

For the ocean heat content changes below 700 m, there is no reliable in-situ global deep ocean data before the Argo observations whose spatial coverage over the global ocean reached a mature state only around 2004-2005. Since there is no reliable global deep ocean observation data for the study period (1971-2012), the ocean heat content changes below 700 m were not explored in this study.

It should be also noted that the OHC_{700} derived from WOA13 increased sharply during 2001-2003 in all ocean basins including the Atlantic and Southern Oceans (Figs. 1 and S2). Previous studies have suggested that the changes in the historical observation network from a ship-based system to Argo floats introduced an artificial jump in OHC_{700} during the initiation of the global Argo array (2001-2003)[2,3,4]. Therefore, the OHC_{700} changes derived from WOA13 during 2001-2003 were not used in this study.

S.I.2. Recent OHC_{700} changes and heat budget for the Atlantic and Southern Oceans

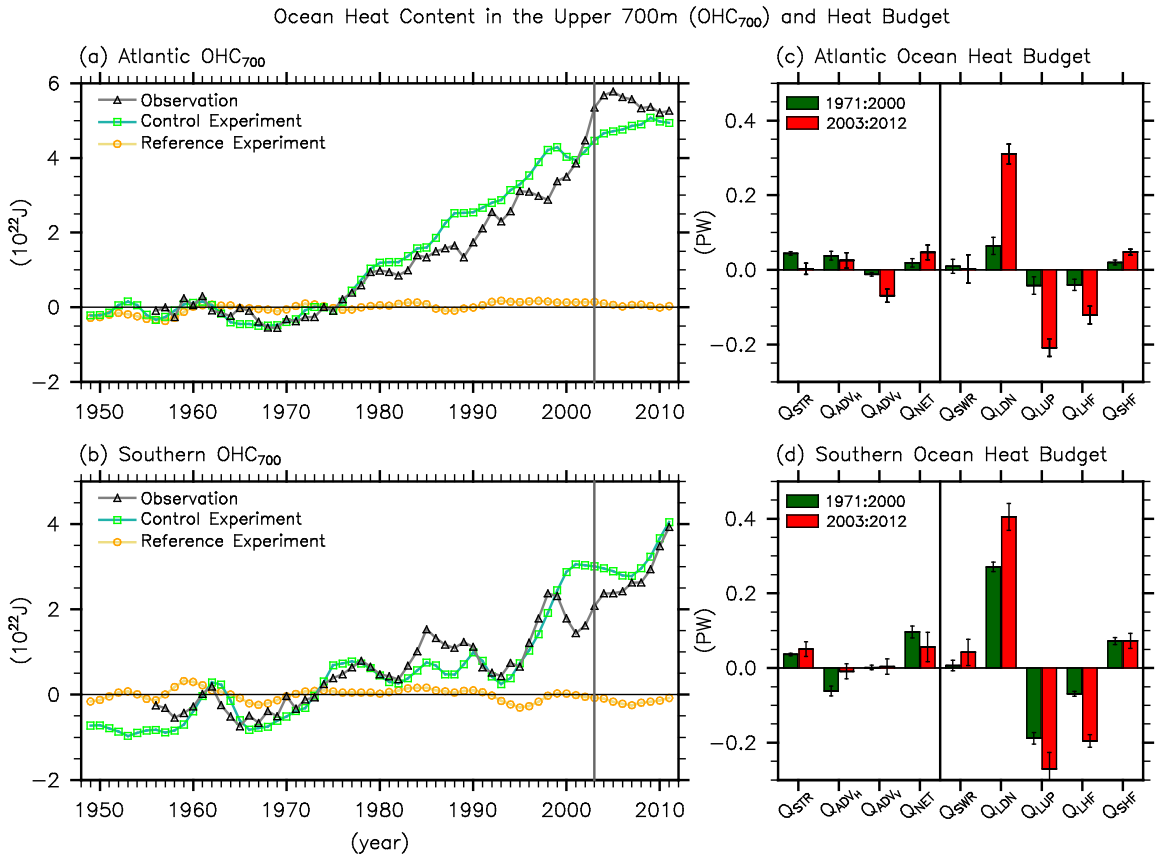

Figure S2. OHC_{700} and heat budget for the Atlantic and Southern Oceans. Time series of OHC_{700} for (a) the Atlantic and (b) Southern Oceans derived from the control and reference experiments and observations[12] are shown. The heat budget terms, namely the storage rate (Q_{STR}), horizontal and vertical advections (Q_{ADV_H} and Q_{ADV_V}), net surface heat flux (Q_{NET}), shortwave radiation (Q_{SWR}), downward and upward longwave radiations (Q_{LDN} and Q_{LUP}), latent heat flux (Q_{LHF}) and sensible heat flux (Q_{SHF}), for (c) the Atlantic and (d) Southern Oceans derived from the control experiment relative to the reference experiment are averaged for the 1971-2000 (green bars) and 2003-2012 periods (red bars). The error bars show the 90 % confidence levels derived from the six-member ensemble runs.

Overall, the control experiment reasonably well captured the observational estimates of OHC_{700} changes in the Atlantic and Southern Oceans since the 1970s (Figs. S2a and S2b). As discussed in S.I.1, however, the OHC_{700} derived from WOA13 increased sharply during 2001-2003 in the Atlantic and Southern Oceans likely due to the changes in historical observation network from a ship-based system to Argo floats[2,3,4]. The simulated OHC_{700} from the control experiments does not show such a sharp increase during this period either in the Atlantic Ocean or in the Southern Ocean.

DOI: 10.1038/NGEO2438

In the Atlantic Ocean, the surface heat uptake increased considerably during 2003-2012 in comparison to the earlier period of 1971-2000. However, a large portion of the anomalous surface heat uptake was transported to the deeper ocean below 700 m ($Q_{ADV_v} < 0$), consistent with previous studies[5,6]; thus, the OHC_{700} did not increase much during 2003-2012 (Figs. S2a and S2c).

In the Southern Ocean, the surface heat uptake reduced somewhat during 2003-2012 in comparison to the earlier period of 1971-2000. Nevertheless, the OHC_{700} did increase during 2003-2012 with a slightly higher rate than that during 1971-2000 (Figs. S2b and S2d) mainly because the southward heat transport into the Southern Ocean across 34° (mainly from the Indian Ocean; see Table S6) increased during 2003-2012 in comparison to the earlier period of 1971-2000.

Additionally, there was no significant transport of heat to the deeper Southern Ocean disagreeing with previous studies[5,6]. However, since there is no reliable in-situ deep ocean data in the Southern Ocean for the study period (1971-2012) and the current state-of-the-art ocean-sea ice models in general have difficulties in reproducing the climatology in the Southern Ocean[7], the heat budget analysis result for the Southern Ocean and its implication for the deeper Southern Ocean should be interpreted with caution.

S.I.3. Discussion on the bias-corrected 20CR surface flux fields

In order to minimize potential biases in the 20CR surface flux fields (see ref 8), the monthly climatologies and high-frequency variability of the 20CR surface flux fields were corrected using the surface flux fields derived from the common ocean-ice reference experiments version 2 (CORE2; ref 9), which is a global surface flux data set corrected by using available observations.

We first constructed a set of monthly surface flux climatologies using the 20CR surface flux variables for 1984-2006, and another set of monthly surface flux climatologies using the CORE2 surface flux variables for the same period. Then, the differences between the two sets of climatologies (i.e., CORE2 - 20CR) were added to the 20CR surface forcing fields.

After correcting the monthly climatologies in the 20CR surface flux variables, a 5-day high-pass filter was applied to the CORE2 surface flux fields to obtain high-frequency variability in the CORE2 surface flux fields. Similarly, a 5-day low-pass filter was applied to the above processed 20CR surface forcing fields to remove high-frequency variability. Then, for each model year (from 1948 to 2012), the high-pass filtered CORE2 surface flux fields for a randomly selected year during 1984-2006 were added to the low-pass filtered 20CR surface flux fields to construct the bias-corrected 20CR surface flux fields.

S.I.4. Discussion on the spin-up run

It is a common practice to spin up an ocean model with a seasonally varying climatological surface flux data set. However, recent studies have suggested that weather noise (linked to winter storms for example) and interannual-frequency surface forcing (linked to the North Atlantic Oscillation for example) are also important in shaping the mean state of the global ocean[10]. The spin-up method with randomly selected forcing years used in this study[11] (Method) conserves the

total variance of the surface flux fields without introducing spurious long-term variability. Therefore, it is an effective way to spin up any ocean or ocean-sea ice coupled models.

S.I.5. Discussion on the heat budget analysis

The heat budgets summarized in Figs. 1 and S2 were obtained by first integrating the heat budget terms derived from the control experiment for the global ocean and for the individual major ocean basins. The spatially integrated heat budget terms for the global ocean and for the individual ocean basins were then averaged for the 1971-2000 and for 2003-2012 periods. The same procedure was used to compute the corresponding heat budget terms from the reference experiment, which were later subtracted from those derived from the control experiment. Therefore, the heat budget terms shown in Figs. 1 and S2 are the time-averaged values for the 1971-2000 and 2003-2012 periods in the control experiment relative to the reference experiment.

The heat budget values obtained from the control experiment for 1971-2000 and 2003-2012, the 30-year mean and 10-year mean of the reference experiment, and the differences (control experiment for 1971-2000 minus 30-year mean of the reference experiment; control experiment for 2003-2012 minus 10-year mean of the reference experiment) are summarized in Table S2, S3, S4, S5 and S6 for the global ocean and for the Indian, Pacific, Atlantic and Southern Oceans, respectively. The heat budget values for the control experiment are based on the 6-member ensemble averages. For the reference experiment, the 6-member ensemble averages of the 424-453, 524-553, 624-653, 724-753, 824-853, and 924-953 model years were used to obtain the 30-year mean heat budget values. Similarly, the 6-member ensemble averages of the 456-465, 556-565, 656-665, 756-765, 856-865, and 956-965 model years were used to obtain the 10-year mean heat budget values.

Table S2. **Heat budget for the global ocean in the upper 700 m**. The heat budget terms for the global ocean in the upper 700 m derived from the control experiment for 1971-2000 and 2003-2012, the 30-year mean and 10-year mean of the reference experiment and the differences (control experiment for 1971-2000 minus 30-year mean of the reference experiment; control experiment for 2003-2012 minus 10-year mean of the reference experiment) are shown. The unit is PW.

Heat budget terms	1971-2000			2003-2012		
	Control	Reference	Control – Reference	Control	Reference	Control – Reference
Q_{STR}	0.10	0.00	**0.10**	0.12	0.01	**0.11**
Q_{NET}	0.12	-0.02	**0.15**	0.19	-0.03	**0.23**
Q_{SWR}	59.51	59.34	**0.17**	59.46	59.36	**0.10**
Q_{LHF}	-34.10	-33.75	**-0.35**	-34.48	-33.76	**-0.72**
Q_{SHF}	-5.41	-5.57	**0.16**	-5.30	-5.58	**0.28**
Q_{LDN}	123.34	122.75	**0.58**	124.17	122.72	**1.45**
Q_{LUP}	-143.11	-142.69	**-0.42**	-143.56	-142.68	**-0.88**
Q_{ADV_v}	-0.02	0.02	**-0.04**	-0.08	0.04	**-0.12**

DOI: 10.1038/NGEO2438

Table S3. Heat budget for the Indian Ocean in the upper 700 m. Same as Table S2, except for the Indian Ocean.

Heat budget terms	1971-2000			2003-2012		
	Control	Reference	Control – Reference	Control	Reference	Control – Reference
Q_{STR}	0.00	0.00	**0.00**	0.07	0.00	**0.07**
Q_{NET}	0.13	0.11	**0.02**	0.11	0.12	**-0.01**
Q_{SWR}	9.55	9.49	**0.06**	9.57	9.51	**0.06**
Q_{LHF}	-5.99	-5.88	**-0.11**	-6.10	-5.88	**-0.22**
Q_{SHF}	-0.64	-0.68	**0.03**	-0.63	-0.68	**0.05**
Q_{LDN}	17.89	17.81	**0.07**	18.01	17.81	**0.12**
Q_{LUP}	20.68	-20.65	**-0.03**	-20.74	-20.65	**-0.09**
Q_{ADV_H} (SOC to IND)	-1.11	-1.12	**0.01**	-1.18	-1.11	**-0.07**
Q_{ADV_H} (PAC to IND)	0.96	0.97	**-0.01**	1.14	0.95	**0.19**
Q_{ADV_V}	0.02	0.04	**-0.01**	0.00	0.04	**-0.04**

Table S4. Heat budget for the Pacific Ocean in the upper 700 m. Same as Table S2, except for the Pacific Ocean.

Heat budget terms	1971-2000			2003-2012		
	Control	Reference	Control – Reference	Control	Reference	Control – Reference
Q_{STR}	0.02	0.00	**0.02**	-0.02	0.00	**-0.02**
Q_{NET}	0.82	0.81	**0.02**	0.93	0.79	**0.13**
Q_{SWR}	26.32	26.25	**0.08**	26.22	26.26	**-0.04**
Q_{LHF}	-15.63	-15.50	**-0.13**	-15.69	-15.52	**-0.18**
Q_{SHF}	-2.08	-2.12	**0.04**	-2.01	-2.12	**0.11**
Q_{LDN}	52.31	52.21	**0.10**	52.57	52.21	**0.36**
Q_{LUP}	-60.08	-60.01	**-0.07**	-60.14	-60.01	**-0.13**
Q_{ADV_H} (SOC to PAC)	0.24	0.23	**0.01**	0.27	0.22	**0.06**
Q_{ADV_H} (IND to PAC)	-0.96	-0.97	**0.01**	-1.14	-0.95	**-0.19**
Q_{ADV_V}	-0.09	-0.07	**-0.02**	-0.08	-0.06	**-0.02**

Table S5. Heat budget for the Atlantic Ocean in the upper 700 m. Same as Table S2, except for the Atlantic Ocean.

Heat budget terms	1971-2000			2003-2012		
	Control	Reference	Control – Reference	Control	Reference	Control – Reference
Q_{STR}	0.05	0.00	**0.04**	0.00	0.00	**0.00**
Q_{NET}	-0.31	-0.33	**0.02**	-0.29	-0.34	**0.05**
Q_{SWR}	12.72	12.71	**0.01**	12.72	12.72	**0.00**
Q_{LHF}	-7.57	-7.53	**-0.04**	-7.66	-7.54	**-0.12**
Q_{SHF}	-1.176	-1.20	**0.02**	-1.15	-1.20	**0.05**
Q_{LDN}	25.42	25.36	**0.06**	25.67	25.36	**0.31**
Q_{LUP}	-29.65	-29.60	**-0.04**	-29.81	-29.61	**-0.22**
Q_{ADV_H} (SOC to ATL)	0.65	0.61	**0.04**	0.63	0.61	**0.03**
Q_{ADV_V}	-0.29	-0.28	**-0.01**	-0.34	-0.27	**-0.07**

Table S6. Heat budget for the Southern Ocean in the upper 700 m. Same as Table S2, except for the Southern Ocean.

Heat budget terms	1971-2000			2003-2012		
	Control	Reference	Control – Reference	Control	Reference	Control – Reference
Q_{STR}	0.04	0.00	**0.04**	0.06	0.00	**0.05**
Q_{NET}	-0.46	-0.56	**0.10**	-0.50	-0.56	**0.06**
Q_{SWR}	10.54	10.54	**0.01**	10.58	10.54	**0.04**
Q_{LHF}	-4.66	-4.59	**-0.07**	-4.78	-4.58	**-0.20**
Q_{SHF}	-1.38	-1.45	**0.07**	-1.38	-1.45	**0.07**
Q_{LDN}	26.20	25.93	**0.27**	26.33	25.92	**0.40**
Q_{LUP}	-30.91	-30.72	**-0.19**	-30.99	-30.72	**-0.27**
Q_{ADV_H} (ATL to SOC)	-0.65	-0.61	**-0.04**	-0.63	-0.61	**-0.03**
Q_{ADV_H} (IND to SOC)	1.11	1.12	**-0.01**	1.18	1.11	**0.07**
Q_{ADV_H} (PAC to SOC)	-0.24	-0.23	**-0.01**	-0.27	-0.22	**-0.06**
Q_{ADV_V}	0.28	0.28	**0.00**	0.29	0.28	**0.00**

As shown in Tables S3 and S4, the inter-ocean heat transport from the Pacific to the Indian Ocean via the Indonesian passages greatly increased during 2003-2012 (~ 0.19 PW). During the same period, the southward heat transport from the Indian Ocean to the Southern Ocean across 34ºS increased (~ -0.07 PW; the negative indicates transport from the Pacific Ocean to the Indian Ocean) and thus slightly decreased the heat gain from the Pacific Ocean. In the Pacific Ocean, the increased inter-ocean heat transport from the Pacific to the Indian Ocean (~ -0.19 PW; the negative indicates transport from the Pacific Ocean to the Indian Ocean) was somewhat compensated by the increased northward heat transport from the Southern Ocean to the Pacific Ocean across 34ºS (~ 0.06 PW).

S.I.6. Discussion on the three sensitivity experiments

Additional sensitivity experiments (Methods) were carried out to further understand the relative importance of wind forcing from the different ocean basins in driving the ITF variability. Using real-time surface winds *inside* the Pacific Ocean and climatological winds *outside* of the Pacific Ocean (EXP_PAC), the abrupt increase of the Indian OHC_{700} during the 2000s was successfully simulated, whereas ensemble runs forced by real-time surface winds *inside* the Southern Ocean and climatological surface winds *outside* of the Southern Ocean (EXP_SOC) almost completely failed to reproduce the Indian OHC_{700} increase in the 2000s (Fig. 4a).

Using real-time surface winds *inside* the Indian Ocean and climatological surface winds *outside* of the Indian Ocean (EXP_IND), the ensemble runs captured the Indian OHC_{700} increase, although only a small fraction of it (Fig. 4a). In both EXP_PAC and EXP_IND, the heat budget also indicates that the inter-ocean heat transport carried by the ITF increased during 2003-2012, albeit more so in EXP_PAC than in EXP_IND (Fig. 4c). Therefore, these sensitivity experiments confirm that the anomalous surface wind fields in the Pacific and Indian Oceans are the key to increasing the ITF heat transport in the control experiment during 2003-2012.

References

1. Levitus, S., Antonov, J. I., Boyer, T. P., Locarnini, R. A., Garcia, H. E. & Mishonov A. V. Global ocean heat content 1955–2008 in light of recently revealed instrumentation problems. *Geophys. Res. Lett*. **36,** L07608 (2009).

DOI: 10.1038/NGEO2438

2. Cheng, L. & Zhu, J. Artifacts in variations of ocean heat content induced by the observation system changes. *Geophys. Res. Lett*. **41**, 7276–7283 (2014).
3. Lyman, J. M. & Johnson, G. C. Estimating global ocean heat content changes in the upper 1800 m since 1950 and the influence of climatology choice. *J. Clim*. **27**, 1945–1957 (2014).
4. Balmaseda, M. A., Trenberth, K. E., & Källén, E. Distinctive climate signals in reanalysis of global ocean heat content. *Geophys. Res. Lett.* **40**, 1754–1759 (2013).
5. Chen, X. & Tung, K.-K. Varying planetary heat sink led to global-warming slowdown and acceleration. *Science* **345**, 897-903 (2014).
6. Drijfhout, S. S., Blaker, A. T., Josey, S. A., Nurser, J. G., Sinha, B. & Balmaseda, M. A. Surface warming hiatus caused by increased heat uptake across multiple ocean basins. *Geophys. Res. Lett*. **41**, 7868–7874 (2014).
7. Weijer, W., Sloyan, B. M., Maltrud, M. E., Jeffery, N., Hecht, M. W., Hartin, C. A., van Sebille, E., Wainer, I. & Landrum, L. The Southern Ocean and its climate in CCSM4. *J. Clim*. **25**, 2652–2675 (2012).
8. Krüger O., Schenk F., Feser F. & Weisse R. Inconsistencies between long-term trends in storminess derived from the 20CR reanalysis and observations. *J. Clim*. 26, 868-874 (2013).
9. Large W. G. &Yeager, S. G. The global climatology of an interannually varying air–sea flux data set. *Clim. Dyn*. **33**, 341-364 (2009).
10. Kirtman, B. P., Bitz, C., Bryan, F., Collins, W., Dennis, J., Hearn, N., Kinter III, J. L., Loft, R., Rousset, C., Siqueira, L., Stan, C., Tomas, R. & Vertenstein, M. Impact of ocean model resolution on CCSM climate simulations. *Clim. Dyn*. **39**, 1303-1328 (2012).
11. Lee, S.-K., Park, W., van Sebille, E., Baringer, M. O., Wang, C., Enfield, D. B., Yeager, S. & Kirtman, B. P. What caused the significant increase in Atlantic Ocean heat content since the mid-20th century? *Geophys. Res. Lett*. **38**, L17607 (2011).